Cell Reports
Physical Science

CellPress
OPEN ACCESS

Article

Thermodynamic analysis of a zero-emission combustion cycle for energy transition

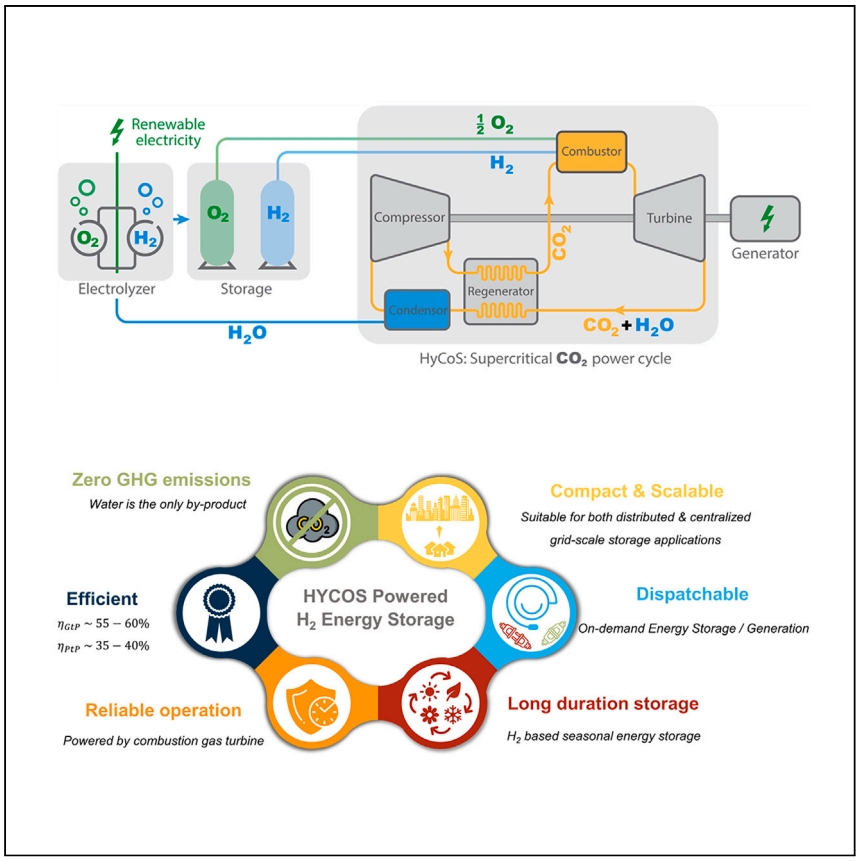

Future energy grids need seasonal storage to absorb renewable variability and enhance flexibility. Dave et al. propose coupling green H_2-based energy storage with HYCOS cycle, a zero-emission combustion cycle. Highly scalable and compact, the HYCOS cycle offers >55% net efficiency at distributed generation level, matching/surpassing fuel-cell and IC engine performance.

Kaushal Dave, Arvind Gangoli Rao

a.gangolirao@tudelft.nl

Highlights

The HYCOS cycle is a zero-emission sCO_2 Brayton cycle fueled by H_2/O_2 combustion

sCO_2 as the working fluid makes HYCOS cycle scalable, compact, and highly efficient

Ideal for distributed electricity production with H_2 in energy storage application

At Net efficiency >55%, HYCOS cycle matches/exceeds fuel cell and IC engine performance

Dave & Gangoli Rao, Cell Reports Physical Science 4, 101514
August 16, 2023
https://doi.org/10.1016/j.xcrp.2023.101514

Cell Reports
Physical Science

CellPress
OPEN ACCESS

Article

Thermodynamic analysis of a zero-emission combustion cycle for energy transition

Kaushal Dave[1] and Arvind Gangoli Rao[1,2,*]

SUMMARY

The power sector accounts for ~40% of global energy-related CO_2 emissions. Its decarbonization by switching to low-carbon renewables is essential for a sustainable future. Existing electrical grids, however, have limited capacity to absorb the variability introduced by these new energy sources and rely largely on natural-gas-based power generation. For deep decarbonization, alternative solutions to increase grid flexibility are needed. Among these, energy storage is expected to have a key role. This paper proposes a unique energy storage and re-conversion system by coupling the hydrogen combustion in supercritical CO_2 (HYCOS) cycle, a zero-emission combustion cycle, with long-term/seasonal energy storage based on green H_2 production. This power cycle is expected to be highly scalable and compact and can deliver power at net electrical efficiency between 55% and 60% at distributed generation levels. Thus, it can be highly competitive with existing solutions such as fuel cells, reciprocating engines, and gas turbines.

INTRODUCTION

The power sector accounts for ~40% of global energy-related CO_2 emissions. Its decarbonization by switching to variable renewable energy sources (VRES) is crucial for sustainability. As a result, a massive integration of VRES in the existing grid is expected over the next few years. Several authors[1–5] have previously investigated the potential challenges arising from such large-scale integration. The two main challenges that are of interest in the context of this analysis are an increase in the grid flexibility requirement and a shift in power generation sector away from a centralized model to a distributed model. Energy storage is expected to have a major role in alleviating the flexibility requirements of future energy grids without the carbon footprint associated with current gas-powered generators. However, most of the technologies currently available are only suitable for short term energy storage. As the share of VRES increases, the fluctuations/variations in generation, and consequently, the energy storage requirements are expected to occur over a longer duration/seasons. Thus, development of viable long-term energy storage technologies is critical to ensure a continued increase in the share of VRES in our energy grids.

Power-to-gas (PtG) technology based on production of green H_2 (and its derivatives) is a potential long-term strategy that can enable deep decarbonization of the future global economy.[6,7] Among other applications, PtG (green H_2) technology can be used for seasonal energy storage application in combination with H_2-based power generation solution. However, these concepts are yet to see widespread adoption because of several challenges associated with their implementation.[7–9] Considering that future power generators are expected to serve the grids in a load balancing mode at distributed generation level, fuel cells with their superior efficiencies

[1]Sustainable Aircraft Propulsion, Flow Physics and Technology Department, Faculty of Aerospace Engineering, Delft University of Technology, Kluyverweg 1, 2629 HS Delft, the Netherlands

[2]Lead contact

*Correspondence: a.gangolirao@tudelft.nl

https://doi.org/10.1016/j.xcrp.2023.101514

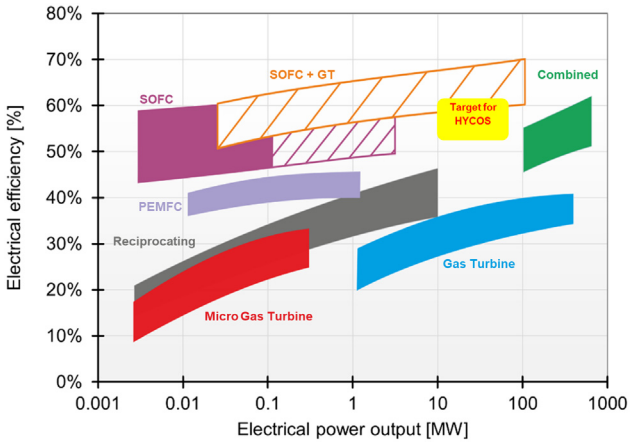

Figure 1. Comparison of the target design space for the HYCOS cycle with several options currently available in the power generation market

This plot is inspired by the Horizon 2020 Bio-HyPP project.

have an edge over the existing combustion-based power cycles. However, bulk power generation using fuel cells has several operational disadvantages including high operating and maintenance (O&M) costs, limited stack lifetime, poor load following capabilities, low power density, performance stability, and unreliable operational characteristics at high operating temperatures. On the other hand, combustion-based power generation technologies have favorable operational characteristics but have substantially lower efficiencies when scaled down to distributed generation level. This dichotomy between fuel-cell systems and combustion-based power cycles highlights a technological gap in the distributed power generation market. This is shown as the target design space in Figure 1. There is a need for a combustion-based cycle that can offer efficiencies competitive with fuel cells while having the operational characteristics of conventional power generation systems such as gas turbines/internal combustion (IC) engines.

The performance of a gas turbine is determined by the efficiency of its components and the thermodynamic cycle on which it operates. Although most components of current gas turbine technology have reached their technological limits, a modification to the underlying thermodynamic cycle has the potential to unlock significant efficiency gains in the gas turbine. Re-designing the Brayton cycle to operate in the transcritical/supercritical regime can enhance its performance by using the thermophysical properties of the working fluid near its critical point. This improvement is mainly because fluids near their critical point have high density and low compressibility, which significantly reduces the compression work required for the cycle. Additionally, supercritical fluids have higher heat capacities, making them more effective at recovering waste heat from turbine exhaust in a recuperator. Conventional Brayton cycle uses air as the working fluid and therefore it would have to be operated at cryogenic temperatures to achieve supercritical phase, making it impractical. CO_2, on the other hand, has its critical point at 73.8 bar and ~304 K and therefore, can be used as the working fluid in a supercritical Brayton cycle.

The idea of supercritical CO_2 (sCO_2) Brayton cycle has a long history of development[10–15] for wide ranging application such as nuclear power generation, waste heat recovery, solar thermal power plants, etc. In more recent years, a variation of the sCO_2 Brayton cycle was proposed by Allam et al.[16] The Allam cycle is a

semi-closed, internally fired, natural gas-fueled oxy-fuel combustion sCO_2 power cycle with post-combustion capture of CO_2. This cycle was conceptualized to replace conventional grid-scale power generation technologies, mainly gas-fired combined cycle power plants. Zhou et al.[17] have also proposed the use of the Allam cycle in their compressed CO_2 energy storage (CCES) system. The main disadvantage of the Allam cycle stems from its requirement of using an air separation unit (ASU) to provide the oxidizer for its oxy-fuel combustion process. This reduces its compactness and scalability while increasing the initial cost of investment significantly, which ultimately makes it unsuitable for application at distributed generation levels.

In this paper we propose a compact and scalable variation of the sCO_2 Brayton cycle called hydrogen combustion in sCO_2 (HYCOS) cycle. It is an intercooled, recuperated sCO_2 Brayton cycle fueled with oxy-combustion of hydrogen. Results from the thermodynamic and combustion analysis of this cycle are presented in the subsequent section of the paper. Additionally, results from a gradient-based optimization of the HYCOS cycle are also included. These results show that the HYCOS cycle offers electrical efficiency in the range of 55%–60%, which is comparable with fuel cells at distributed generation levels while still having the operational characteristics of a gas turbine. Additionally, the choice of using an H_2/O_2 combustion system ensures an emission free operation. The cycle has only condensed water as the by-product, which could be reused during H_2 production or other onsite applications. All these characteristics makes the HYCOS cycle an ideal solution not only for the energy storage and re-conversion application, but also for hydrogen-based generation of shaft work/electrical power in the context of distributed energy islands. The schematic shown in Figure 2 is the conceptual representation of the proposed HYCOS cycle.

RESULTS

Univariate parametric analysis of the HYCOS cycle

In theory, an ideal Brayton cycle can be fully defined by specifying the minimum and maximum cycle pressures (i.e., pressures at the beginning and end of the compression/expansion process) and the temperature of the source and the sink (i.e., temperature at beginning of expansion and compression processes respectively). For a real Brayton cycle, in addition to these four control parameter, other constants defining the efficiencies associated with various cycle processes and the thermodynamic properties of the working fluid have to be included. In this analysis, a similar approach is adopted with one key deviation. The temperature at the end of the expansion process is selected as the control parameter instead of the temperature before expansion. As a result, the turbine inlet temperature (TIT), becomes a dependent variable and is iteratively calculated using the expansion pressure ratio, turbine outlet temperature (TOT) and thermodynamic properties of the flue gas mixture. This deviation was adopted because the maximum temperature and pressure encountered in the recuperator were found to be the most limiting factors from a practical design standpoint. Thus, by selecting an acceptable value of TOT, the user can ensure that the results obtained from the model are inherently valid designs. With this important note, the results of the univariate parametric analysis of the HYCOS cycle are presented in the following subsections.

Effect of turbine inlet pressure

The effect of turbine inlet pressure (TIP) was analyzed in the range of 250–450 bar. The maximum operating pressure of HYCOS cycle is limited by the mechanical design requirements of the recuperator and the hot section of the engine. Several concepts using sCO_2 Brayton cycles, found in literature,[18] have been typically

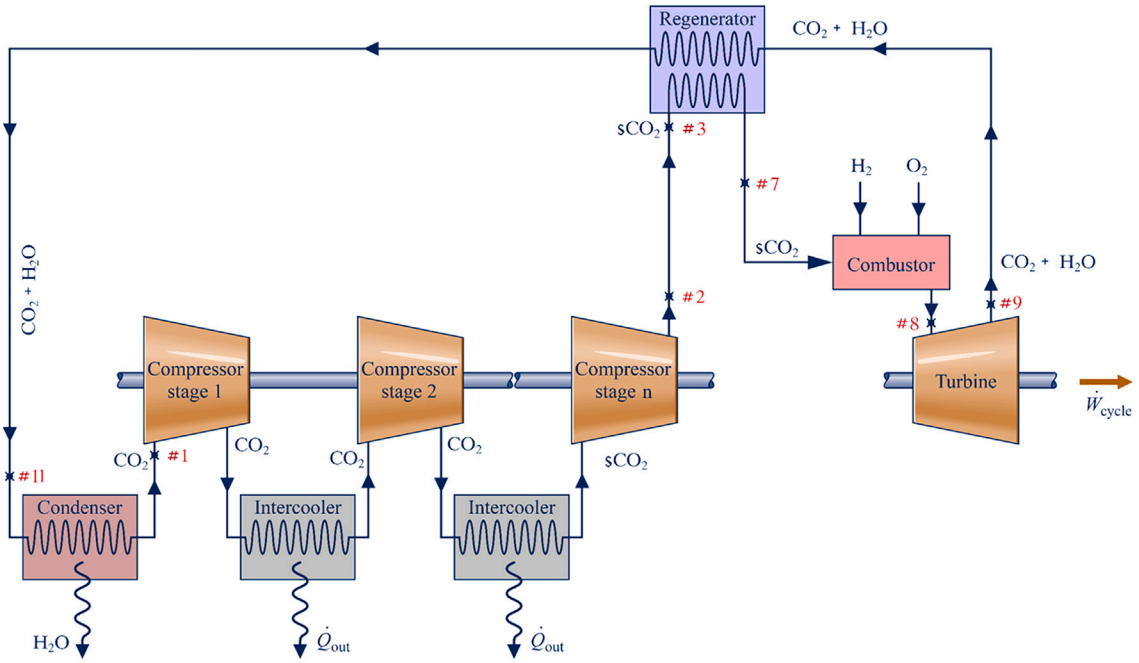

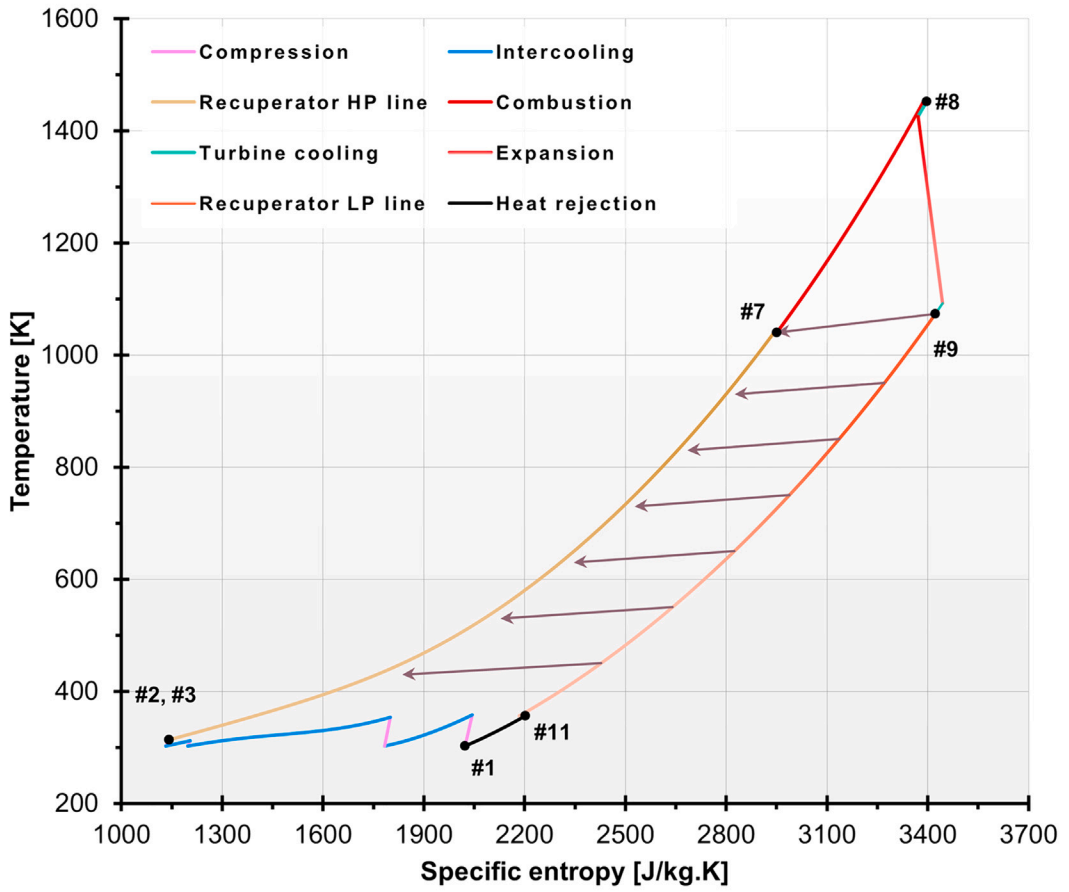

Figure 2. Proposed HYCOS cycle

Schematic layout and T-s chart representation of the proposed HYCOS cycle.

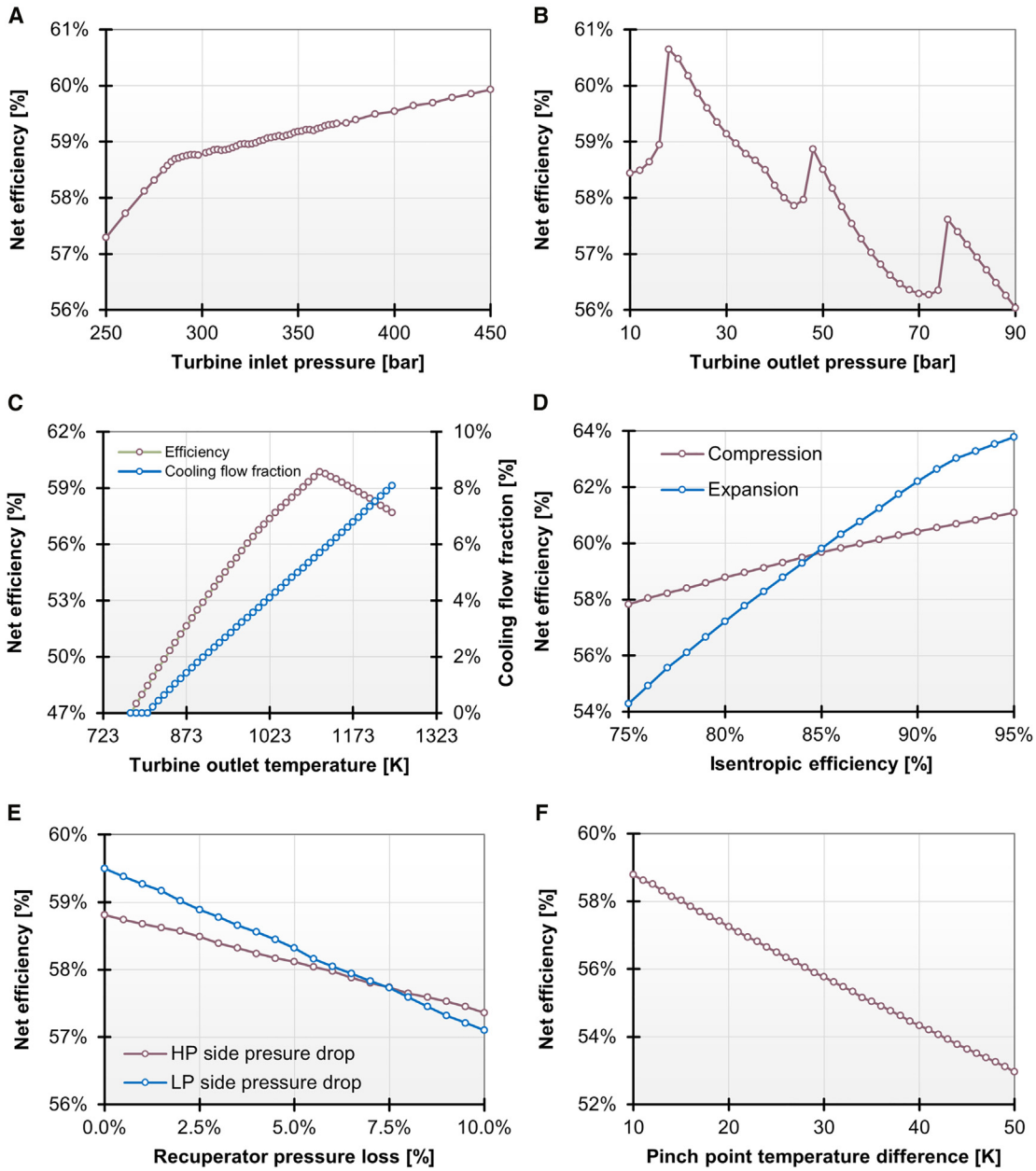

Figure 3. Results of the univariate parametric analysis of the HYCOS cycle

(A) Effect of turbine inlet pressure on the net cycle efficiency.

(B) Effect of turbine outlet pressure on the net cycle efficiency.

(C) Effect of turbine outlet temperature on the net cycle efficiency and turbine cooling flow fraction.

(D) Effect of isentropic efficiency of expansion and compression on the net cycle efficiency.

(E) Effect of HP-side and LP-side pressure loss in recuperator on the net cycle efficiency.

(F) Effect of pinch-point temperature difference on the net cycle efficiency.

proposed with maximum pressures in the range of 300–350 bar. The higher upper limit of TIP in this analysis is selected to theoretically study the thermodynamic behavior of the proposed power cycle. The results obtained are shown in Figure 3A. It can be seen that the net cycle efficiency increases with increasing TIP. This effect can be explained by the fact that increase in TIP results in an increase in the cycle pressure ratio and TIT (from 1,420 K at 250 bar to 1,537 K at 450 bar). An increase

in TIP and TIT results in two opposing effects on the cycle efficiency. On one hand, the net specific work output of the cycle increases, which has a positive impact on the efficiency. On the other hand, an increase in TIT causes the turbine cooling flow requirement and the fuel burn in the combustor to increase, which has a detrimental effect on the cycle efficiency. In the range of this analysis, the increase in net specific work output of the cycle is seen to be more a dominant effect resulting in an increase of the net cycle efficiency with TIP. This behavior is consistent with that of a conventional Brayton cycle.

Effect of turbine outlet pressure

The effect of turbine outlet pressure (TOP) was analyzed in the range of 10–90 bar to study the performance of the HYCOS cycle as it operates in transcritical and supercritical regimes. The results obtained are shown in Figure 3B. The observed variation in net cycle efficiency was ~4.5% with the general trend being that it decreases with an increase in TOP. Similar to the previous case, this can be understood by considering the effect of increasing TOP. As TOP increases, the expansion pressure ratio decreases, which in turn decreases TIT. A reduction in expansion pressure ratio and TIT reduces the net specific work output of the cycle. Although a reduction in TIT also decreases the turbine cooling flow requirement and the fuel burn, the effect of reduction in net specific work output dominates and leads to a reduction in the net efficiency.

Interestingly, on top of this global decreasing trend, Figure 3B shows intermittent peaks. This is caused by the changes in physical properties of the working fluid as it goes from subcritical to supercritical state. As the TOP increases, the compressor inlet pressure also increases and as a result, the compression process shifts more toward the dense phase region causing the compression work requirement to decrease. The spikes observed in Figure 3B are caused when a complete compression step shifts from subcritical to supercritical region.

Effect of TOT

During cycle design, TOT will be limited by the mechanical design consideration for the recuperator and thus it is one of the most constraining design parameter for the HYCOS cycle. The dependence of cycle efficiency on TOT is analyzed in the range of 500°C–950°C. The results obtained are shown in Figure 3C. An increase in TOT first increase and then decrease the net cycle efficiency, which suggests there are competing effects of varying TOT. The first effect of increasing TOT is the corresponding increase in TIT. Second, an increase in TOT results in an increase in the heat rejected at the turbine outlet, which is subsequently recovered in the recuperator and leads to an increase in combustor inlet temperature. Higher TIT increases thermodynamic efficiency of the cycle by increasing the net specific work output. But an increased TIT also leads to an increased fuel consumption and turbine cooling flow. The increase in fuel consumption is partly offset by the increased heat recuperation. In case of an "uncooled" turbine, an increasing TOT for a given cycle pressure ratio (thus increasing TIT) would increase the expansion work of the turbine and thereby always increase the net cycle efficiency. However, in case of real gas turbines, it would result in an increased turbine cooling flow requirement, which has a detrimental effect on the expansion work of the turbine and also the net cycle efficiency. Therefore, overall effect of increasing TOT on the cycle efficiency is dependent on the relative magnitudes of the thermodynamic advantage (because of a higher TIT) and the detrimental effect (because of increased cooling flow requirement). The resulting trend is seen in Figure 3C. This behavior is a typical feature of a Brayton cycle and for any given cycle pressure ratio, an optimum range of turbine inlet and outlet temperatures will exist.

Effect of compression and expansion isentropic efficiency

Component efficiencies have a major impact on the overall efficiency of the Brayton cycle. The isentropic efficiency of compression/expansion process was varied in the range of 75%–95% and the resulting values of net cycle efficiency are plotted in Figure 3D. Unlike, a conventional gas turbine, the effect of isentropic efficiency of expansion on the net cycle efficiency was found to be much larger than the effect of isentropic efficiency of the compressor. This is due mainly to the lower back-work ratio (BWR) for the HYCOS cycle compared with conventional Brayton cycle. Thus, the net output, and as a result the cycle efficiency, of the HYCOS is more sensitive to the efficiency of the expansion process in comparison to that of the compression process. This feature is expected to have a favorable impact on scalability of the HYCOS cycle and will be discussed further in the subsequent section.

Effect of recuperator pressure loss

Pressure losses occurring in the power cycle, although inevitable, are a major cause of loss of cycle efficiency. Therefore, its effect was analyzed by varying the recuperator pressure drop from 0% to 10%. Pressure drop across both the low-pressure (LP) and the high-pressure (HP) streams were varied individually to study the extent of their effect on the net cycle efficiency. The result of this analysis is plotted in Figure 3E. It can be seen that the LP-side pressure drop affects the cycle efficiency more adversely as compared with the HP-side pressure drop. This is caused mainly by the fact that LP-side pressure drop reduces the pressure at vapour phase compressor (VPC) inlet, while the HP-side pressure drop increases the delivery pressure requirement at dense phase compressor (DPC) outlet. The work requirement of the VPC is substantially higher than the DPC and thus, pressure drop on the LP side reduces the net output of the cycle much more than an equivalent pressure drop on the HP side. Thus, the potential impact of any pressure loss occurring on the LP side is substantially larger than the same pressure loss occurring on the HP side.

Effect of recuperator performance

Last, the effect of recuperator performance on the net cycle efficiency was analyzed by varying the pinch-point temperature difference (PPTD) in the range of 10–50 K. The corresponding values of cycle efficiency are plotted in Figure 3F. As the recuperator PPTD increases, the heat recovery from the flue gas stream decreases which reduces the temperature of the recycle stream of sCO_2 at the combustor inlet. This increases the amount of fuel used in the combustor to reach the desire value of TIT, thereby decreasing the net cycle efficiency.

Performance map of the HYCOS cycle

In this section, we analyze the combined effect of two key cycle parameters, TOP and TIT, on the performance of the HYCOS cycle. The authors chose to vary these parameters while keeping the TIP and compressor inlet temperature constant at 300 bar and 302.15 K, respectively. The decision is based on the rationale that, from a designer's perspective, the choice of these parameters will be restricted by the mechanical design limitations and the prevailing ambient condition respectively. In addition to this, PPTD of minimum 10 K was maintained in the recuperator throughout the analysis. The variation of net cycle efficiency, the TOT and the net specific work are plotted in the performance map shown in Figure 4. It is important to consider that because of the large number of computations required for mapping the performance of the HYCOS cycle over a wide design space, the heat exchange process was computed using a limited resolution of 50 intermediate steps. Thus, the performance map provides only a first-level estimate of net cycle efficiency. Although these data can guide the selection of an initial design of the HYCOS cycle during the optimization process, it

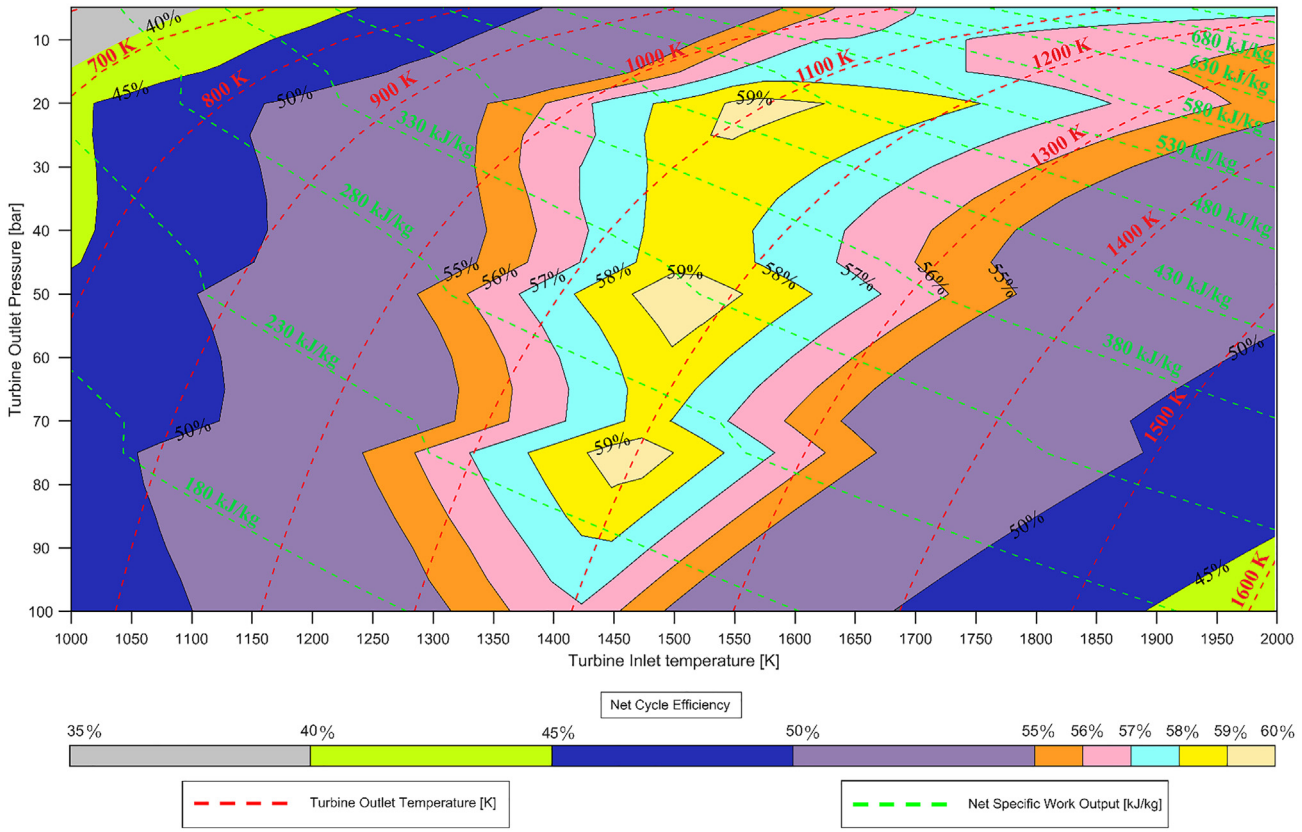

Figure 4. Performance map of the HYCOS cycle

(A–C) Performance map showing (A) net cycle efficiency (contour plot), (B) turbine outlet temperature (red dashed lines), and (C) net specific work output of the cycle (green dashed lines) as a function of turbine outlet pressure and turbine inlet temperature.

should be noted that it does not represent the fully optimized performance of the cycle. More details about the effect of the number of heat exchange steps considered in the recuperator on the estimated cycle efficiency has been discussed in Figure S2 and can be found in supplemental experimental procedures.

Results of cycle optimization

In this section, the results of performing gradient-based optimization on the HYCOS cycle are presented. This optimization was performed using FMINCON solver from MATLAB's Optimization Toolbox. A gradient-based optimizer is prone to converge to local optima in the design space and therefore several optimization with varying initial conditions were performed. Within a thermodynamic context, efficiency optimization of Brayton cycle is fundamentally a 4-dimensional optimization problem. By defining the values of the highest and the lowest cycle temperatures and pressures, the optimization problem can be fully defined. Of these four design variables, choice of the lowest cycle temperature is mainly a function of the sink temperature which in most applications is the ambient temperature. Hence, the optimization problem can then be reduced to a 3-dimensional problem by fixing the lowest temperature (compressor inlet temperature) to a fixed value. The commonly used value for this in literature is 302.15 K[19,20] and the same will be used in this analysis. Next to the choice of design variables, an optimization problem requires definition of bounds, constraints, and optimization constants; these values are defined in Table 1. The cycle configuration with the highest

Table 1. List of parameters used during optimization of the HYCOS cycle

Parameter	Value	Type
Turbine inlet pressure, bar	$150 \leq TIP \leq 300$	bounded variable
Turbine outlet pressure, bar	$5 \leq TOP \leq 100$	bounded variable
Turbine inlet temperature, K	$998.15 \leq TIT \leq 1{,}998.15$	bounded variable
Pinch-point temperature difference, K	$PPTD \geq 10$	constraint
Turbine outlet temperature, K	$TOT \leq 1{,}073.15$	constraint
Compressor inlet temperature, K	302.15	constant
Combustor pressure recovery ratio	0.99	constant
HP-side pressure recovery ratio	0.9973	constant
LP-side pressure recovery ratio	0.97	constant
#Steps in intercooled compression	4	constant
Compression isentropic efficiency, %	80	constant
Expansion isentropic efficiency, %	83	constant
Combustion efficiency, %	99.5	constant
Max allowable blade temperature, K	1,073.15	constant
Turbine cooling model constant μ_c	0.08	constant
Turbine cooling model constant β	0.9	constant
Turbine cooling model constant φ_∞	0.9	constant

efficiency obtained through this optimization process is tabulated and compared with the baseline cycle configuration in Table 2. The increased efficiency of the optimized cycle can be ascribed to an increase of pressure ratio across the turbine and its inlet temperature. This results in an ~38% increase in the specific work output of turbine while the compressor work increases by ~44% compared with the baseline cycle. Nonetheless, as the absolute increase in turbine work is greater than the increase in compressor work, the net specific work output of the cycle increases by ~37%. An increase in TIT also increases fuel burn and the cooling flow requirement. However, the overall impact of increased TIT and cycle pressure ratio is positive, resulting in an increase of more than ~2% in the net cycle efficiency.

Having compared the parameters of the optimized cycle with the baseline cycle, it is worthwhile to note that the optimization process identified several design options with cycle efficiency >55% but significantly less aggressive design parameters. Some of these designs are tabulated in Table 3. It can be observed that all the options presented in Table 3 have a lower peak pressure requirement compared with the baseline and the efficiency optimized cycles presented in Table 2. Therefore, from a practical standpoint, they are expected to be less aggressive in terms of turbine and recuperator design requirements. Alternate cycle #1 offers slightly better efficiency and net specific work compared with the baseline cycle but reduces the peak pressure requirement by 40 bar. Alternate cycle #2 reduces the peak pressure to almost half that in the baseline cycle and has slight lower efficiency. But the higher pressure ratio it operates at allows a significantly higher net specific work output compared with the base case. Similarly, alternate cycle #3 could be viewed as a less aggressive version of the efficiency optimized cycle show in Table 2. It offers almost similar improvement in net cycle efficiency and net specific work output over the baseline cycle at a relatively smaller increase in TIT and a decrease in TIP, thus relieving some of the mechanical design requirements. Therefore, it could be considered more favorable than the efficiency optimized cycle from a component design perspective. Last, alternate cycle #4 represents a configuration that has a lower peak pressure requirement but has a very high cycle pressure ratio. This allows TIT comparable with conventional industrial gas turbine engines while

Table 2. Comparison of the baseline cycle with the optimized cycle

Cycle parameter	Baseline cycle	Optimized cycle
Turbine inlet pressure, bar	300	300
Turbine outlet pressure, bar	34	17.45
Turbine inlet temperature, K	1,455	1,588
Turbine outlet temperature, K	1,073	1,073
Specific turbine work, kJ/kg	463	641
Specific compressor work, kJ/kg	93	134
Net specific work output, kJ/kg	371	507
Net cycle efficiency, %	58.8	60.7
Cooling flow fraction, %	5.0	6.7
H_2 maas flow rate, g/s	5.22	6.96

satisfying the exit temperature constraint imposed by the recuperator design requirement. This configuration has a slightly lower net cycle efficiency but has almost twice the net specific work output of the baseline design and therefore could be favorable for compact applications. The key objective of discussing the alternate cycles presented in Table 3 is to show that the HYCOS cycle could be optimized for satisfying design requirements other than highest efficiency like lower peak pressure or higher net specific work output while also maintaining a relative high cycle efficiency.

Results of combustion analysis

The HYCOS cycle features a unique combustion process where H_2/O_2 mixture is combusted at very HPs while using sCO_2 as the process diluent. This type of combustion system is unique and has therefore not been investigated in the literature. As per authors knowledge, the only other application with a similar combustion system is proposed in the work of Zhou et al.[17] but the study does not include any analysis of the combustion process. Preliminary insights into the behavior of this process can be gained from the studies focusing on syngas combustion however, most of these studies are performed at low-to-moderate pressure. In order to understand the chemical kinetics of the proposed combustion process under supercritical operating conditions, a parametric analysis is conducted wherein the effects of combustor inlet pressure, inlet temperature, equivalence ratio, and dilution ratio are studied. The definitions/interpretation of the key terms used to analyze the results are listed here.

- Ignition delay time (τ_{ig}): Residence time needed to observe a temperature rise of 250 K over the combustor inlet temperature, determined using an adiabatic closed batch reactor in Ansys Chemkin Pro.
- Residence time for stabilization (τ_{stab}): Residence time needed to achieve steady state temperature in the flue gas.
- Mixture reactivity: In the present context, the reactivity of the mixture is qualitatively represented by the ignition delay time (τ_{ig}) and the residence time (τ_{stab}) after which the flue gas temperature stabilizes. A reduction in either τ_{ig} or τ_{stab} is interpreted as an increase in mixture reactivity.

The baseline parameters for the combustor are selected from the results of the thermodynamic evaluation of the baseline HYCOS cycle (see Table 2). Both H_2 and O_2 are entirely injected in PSR #1 while CO_2 is injected equally in PSR #1 and PSR #2 (i.e., dilution ratio of 0.5) (explained in the subsequent section). On the basis of a preliminary analysis of the proposed H_2/O_2 combustion in sCO_2 environment, carbon monoxide (CO) and hydroxide ion (OH) are expected to be the most prevalent minor species in the flue gas mixture in addition to a small fraction of unburnt fuel and

Table 3. Alternative configurations of the HYCOS cycle

Cycle parameter	Alternative cycle #1	Alternative cycle #2	Alternative cycle #3	Alternative cycle #4
Turbine inlet pressure, bar	260	160	261.5	235
Turbine outlet pressure, bar	25	6.5	21	5
Turbine inlet temperature, K	1,486	1,661	1,522	1,808
Turbine outlet temperature, K	1,073	1,073	1,073	1,073
Efficiency, %	59.7	57.4	60.5	58.5
Net specific work, kJ/kg	400	548	436	715
Cooling flow fraction, %	5.4%	7.6%	5.8%	9.6%

oxidizer. Therefore, the variation in flue gas composition is discussed in terms of observed levels of CO/H_2/O_2/OH at the exit of PSR #2.

Effect of combustor inlet temperature and pressure

A variation in combustor inlet temperature and pressure was seen to affect both the reactivity and the final composition of the flue gases. Data tabulated in Table 4 and Table 5 show that an increase in combustor inlet temperature and pressure results in the reduction of τ_{ig} and τ_{stab} and thereby increases mixture reactivity. The increase in mixture reactivity with an increase in combustor inlet temperature can be explained using the Arrhenius equation (see Equation 1) that represents the rate constant k in terms of the pre-exponential (frequency) factor A, activation energy E_a, and the temperature T.

$$k = A * e^{-E_a/RT} \quad \text{(Equation 1)}$$

The temperature dependence of rate constant k is attributed mainly to the exponential part of Equation 1. However, the pre-exponential factor A can also be a weak function of temperature and is proportional to T^m with the value of m usually depending on the method or theory used to evaluate it. As temperature increases, the rate constant increases, accelerating the combustion reactions and increasing the reactivity of the mixture as shown in Table 4. It is worth noting that while increasing the combustor operating temperature was expected to enhance endothermic reactions and lead to a higher formation and concentration of intermediate/ionic species such as H, O, OH, and CO in the flue gas mixture, this trend was only observed at extensively long residence times (i.e., when the flue gas composition reached equilibrium). At shorter residence times, a contrary trend was observed as shown in Table 4. This can be explained by considering the coupling between the combustor inlet temperature and the residence time in the combustor. An increase in inlet temperature increases mixture reactivity, pushing the reactions toward chemical equilibrium more quickly. At finite residence times, such as those reported in Table 4, this acceleration toward equilibrium results in lower measured concentrations of intermediate species in the flue gas mixture with increase in combustor inlet temperature. However, this trend reverses if the reactions/flue gas compositions were allowed to reached equilibrium values ($\tau_{res} > 1,000$ ms).

Equation 1 does not show any direct dependence of the rate constant on the pressure, however, the increased mixture reactivity with an increase in combustor pressure seen from Table 5 was attributed to the increase in the third body collision efficiency by Kéromnès et al.[21] This can mainly be because of an increase in pre-exponential (or frequency) factor A triggered by a higher number of effective molecular collisions i.e., an increase in the steric factor. Additionally, in accordance with the Le Chatelier's principle, an increase in combustor pressure tends to reduce

Table 4. Effect of combustor inlet temperature on mixture reactivity and flue gas composition

Inlet temperature, K	τ_{ig}, ms	τ_{stab}, ms	FG temperature, K	CO_2, %	H_2O, %	CO, ppm	H_2, ppm	O_2, ppm	OH, ppm
960	4.84	129	1,444.7	89.13	10.76	387	18	633	1
1,030	1.12	129	1,511.6	89.13	10.78	325	14	534	3
1,040	0.93	129	1,521.1	89.14	10.78	309	13	526	3
1,050	0.77	131	1,530.7	89.14	10.78	288	12	515	4
1,120	0.24	129	1,597.3	89.16	10.77	168	7	516	9

dissociation of CO_2 and pushes the chemical reactions toward completion. This in turn lead to a reduction in τ_{stab} and a reduction in concentration of minor species in the flue gas as evidenced in Table 5.

Effect of dilution ratio

In order to avoid high temperatures in the combustor, the combustion products are diluted with CO_2. The effect of CO_2 dilution on the combustion process is analyzed in this section. The term dilution ratio is defined as the ratio CO_2 entering in PSR #1 to the total amount of CO_2 injected during the combustion process (see Figure S1). In this analysis, all the required fuel and oxidizer are injected in PSR #1 and only the flow of CO_2 is varied. The effect of this variation on the inlet composition of the reactant mixture in PSR #1 is shown in Figure 5A.

As shown in previous studies,[22,23] the dilution of H_2/O_2 combustion reactions with CO_2 has two main effects, it leads to a thermal/physical dilution of the reactant mixture and it changes the reaction kinetics. First, by physically diluting the combustion mixture, CO_2 not only increases the average (bulk) specific heat capacity of the mixture but also increases the total mass flow entering the combustor. This limits the temperature rise observed during the combustion process. Second, CO_2 affects the kinetics of H_2/O_2 combustion by acting as an inhibitor that decreases mixture reactivity and increases the ignition time delay. At lower temperatures, this kinetic effect is caused mainly by higher third body collision efficiency of CO_2, while at higher temperatures, this effect is a result of the binary reactions of CO_2 with H/OH/O ions thereby decreasing the rate of main branching reactions.

Both these phenomena can be clearly observed by examining the plots shown in Figure 5C. As the CO_2 dilution ratio decreases, the overall heat capacity of the mixture entering the combustor reduces (thermal/physical effect of dilution) and thus the bulk temperature in PSR #1 during combustion increases. Also, a reduction in CO_2 dilution ratio increases the mixture reactivity because of increase in temperature and a reduction in the inhibiting effect on chemical kinetics of H_2/O_2 combustion. This effect can be evidenced by the decrease in ignition delay time. In principle, dilution ratio should not affect the final flue gas composition, as no other initial condition is varied except for the diluent flow distribution between the two stages of the combustor. As seen from Figure 5E, this was indeed the case for very long residence times (τ_{res} > 10 s). However, as such long residence times would lead to an impractical design of the combustor and chemical reactions proceed at only a finite rate, the choice of dilution ratio does affect the flue gas composition. As can be seen from Figure 5E, the lower the residence time, the lower is the value of optimum dilution ratio (defined as the dilution ratio needed to minimize CO concentration in flue gas). As the residence time in consideration increases, the overall CO level decreases as the combustion reactions move closer to equilibrium while the value of optimum dilution ratio increases.

Table 5. Effect of combustor inlet pressure on mixture reactivity and flue gas composition

Inlet pressure, bar	τ_{ig}, ms	τ_{stab}, ms	FG temperature, K	CO_2, %	H_2O, %	CO, ppm	H_2, ppm	O_2, ppm	OH, ppm
250	1.06	139	1,520.5	89.14	10.76	319	14	597	3
340	0.86	124	1,520.9	89.15	10.77	238	10	554	3
350	0.84	123	1,520.9	89.15	10.77	230	10	550	3
360	0.83	121	1,521.0	89.15	10.77	225	10	547	3
450	0.71	109	1,521.2	89.16	10.77	177	8	523	3

Effect of equivalence ratio in PSR #1

In this section, the effect of the varying equivalence ratio of reactant mixture in PSR #1 (i.e., distribution of fuel/oxidizer) on the combustion characteristics is analyzed. The equivalence ratio in PSR #1 is varied from 0.6–1.4 in steps of 0.2 while holding the dilution rate constant at 1. This variation was achieved by restricting the flow of H_2 (for achieving lean condition) and O_2 (for achieving rich condition) in PSR #1. The residual flow of H_2 or O_2 was then injected in PSR #2 to maintain the total flow of reactants and the overall equivalence ratio of the process constant. The effect of this variation on the inlet composition of the reactant mixture in PSR #1 is shown in Figure 5B.

A visible effect of varying the equivalence ratio in PSR #1 is the reduction is in the combustion temperature in PSR #1. The trend seen in Figure 5D is consistent with the general behavior of combustion reactions occurring at non-stoichiometric conditions. The reduction in temperature under lean conditions is caused by the fact that heat released in PSR #1 reduces due to reduction in fuel entering in this section. On the other hand, under rich conditions, the reactions are starved by lack of oxygen resulting in a lower temperature in PSR #1. When PSR #1 operates under non-stoichiometric conditions, flue gas enters PSR #2 at temperatures lower than its equilibrium temperature. As the residual flow of fuel/oxidizer (under lean/rich conditions respectively) is added in PSR #2, the combustion reactions continue toward equilibrium while increasing the flue gas temperature to its final value. This can be observed in Figure 5D.

The effect of finite rate combustion chemistry diminishes as the residence time in the combustor increases. Flue gas tends to stabilize to its equilibrium value which is dependent only on the bulk parameters of the combustion system (i.e., combustor inlet temperature, pressure, and the total flow rate of reactants/overall equivalence ratio). As these remain constant during this analysis, the flue gas composition at exceedingly long residence times ($\tau_{res} > 10$ s) has the same order of magnitude in all cases as shown in Figure 5F. However, such long residence times are not feasible for practical applications and are only included as theoretical test cases. Under reasonable conditions, such as (10 ms $< \tau_{res} <$ 100 ms), the flue gas in the stoichiometric case has the lowest concentration of CO. This indicates that the combustion system reaches equilibrium faster at stoichiometric conditions compared with non-stoichiometric cases.

When comparing the concentration of CO in flue gas at exit of PSR #2 under lean and rich conditions in PSR #1, it can be observed that at very short residence times, CO levels under rich conditions are higher. However, as the residence time is progressively increased, these levels reduce and at some point, become lower than the values predicted under lean conditions. In present analysis, this crossover is observed near $\tau_{res} \approx 100$ ms. A possible cause can be that under fuel-rich conditions in PSR #1, CO_2 acts as a source of oxygen and forms substantially more CO. As this

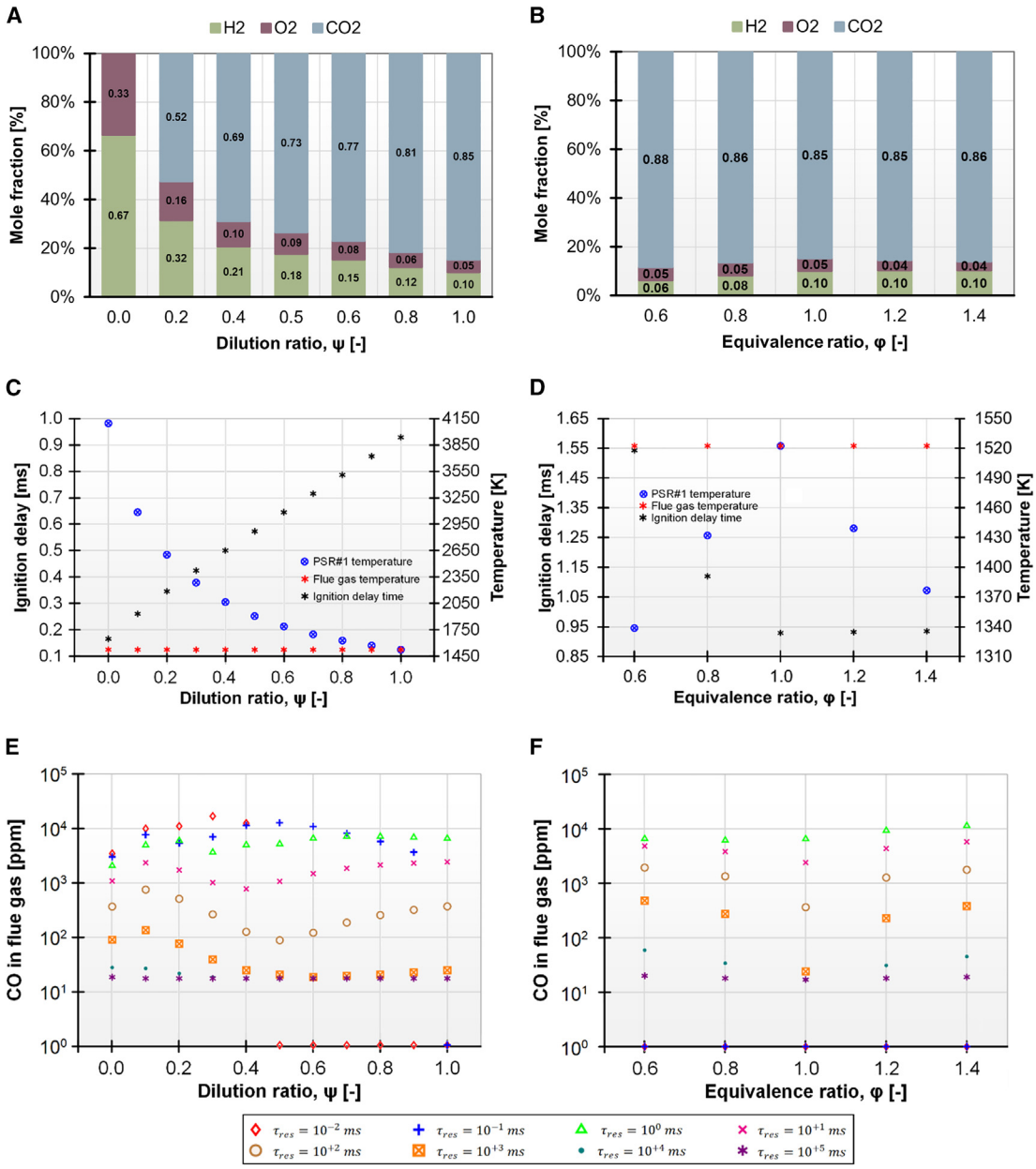

Figure 5. Results of the parametric combustion analysis

(A–F) Effect of varying dilution ratio (A) and equivalence ratio (B) on the reactant composition at the inlet of the combustor. Effect of varying dilution ratio (C) and equivalence ratio (D) on the ignition delay time and combustor temperature. Effect of varying dilution ratio (E) and equivalence ratio (F) on the concentration of CO in flue gas at several residence times, τ_{res}.

product mixture enters PSR #2, it encounters a fresh supply of oxidizer. CO then gets consumed as it reacts with O_2 to form CO_2 as the reactions proceed toward equilibrium. On the contrary, under fuel-lean conditions in PSR #1, there is already an excess supply of oxidizer present and therefore, CO concentration does not increase to very high levels. But as this product mixture enters PSR #2, it encounters fresh supply of fuel, which begins reacting with the products of partial combustion from PSR #1. This results in increasing the CO concentration at shorter residence times which then gets consumed as the reactions proceed toward equilibrium(with increasing

residence times). Therefore, the comparison of the final concentration of CO in PSR #1 under fuel-rich and fuel-lean conditions is dependent on the residence time. At shorter residence times, the final CO levels in flue gases is higher under fuel-rich conditions, while the opposite is true at slightly longer residence times.

DISCUSSION

A zero-emission combustion-based thermodynamic cycle has been proposed which features net electrical efficiency between 55% and 60% at distributed power generation levels. In contrast with conventional Brayton cycle, the net efficiency of the proposed HYCOS cycle was found to be sensitive to turbine isentropic efficiency rather than to the compressor isentropic efficiency. This is expected to have a positive impact on scalability of the cycle since turbines, unlike compressors, operate under a favorable pressure gradient and are easier to scale down with minimum loss of performance. The cycle efficiency was also seen to be more affected by LP-side pressure loss compared with HP-side pressure loss. This was found to be the case because the CO_2 compressor operates under transcritical conditions and compressing subcritical vapor is more expensive than pumping supercritical fluid.

Combustion analysis of the HYCOS cycle showed that the mixture reactivity tends to increase with increasing combustor inlet temperature and pressure. The final concentration of minor products of combustion were found to increase with increasing mixture inlet temperature and decreasing combustor inlet pressure. The study of the effect of relative concentration of $H_2/O_2/CO_2$ (variation in equivalence and dilution ratios) showed that the combustion reactions reached closest to the equilibrium conditions when the reactant mixture was injected at stoichiometric conditions ($\varphi = 1$). Both the fuel and the oxidizer will have to be mixed with CO_2 before combustion to reduce peak flame temperatures. The choice of optimum dilution ratio, therefore, is affected by selection of other parameters like the peak temperature permitted in the combustor and the overall residence time in the combustor. For residence times typically used in industrial gas turbine applications (i.e., 10–50 ms and peak temperature in the combustor limited to ~1,800 K), the optimal range of dilution ratio was found to be 0.6–0.8. This range shifts toward higher values as the residence time increases and the maximum allowable temperature in the combustor decreases. Last, the combustion analysis also showed that the concentration of minor product of combustion and unburnt fuel/oxidizer in the flue gases was sufficiently low to not affect the macro properties of the exhaust gases. Therefore, the simplified treatment of the flue gas mixture as a binary mixture of CO_2 and H_2O during the thermodynamic analysis is justified.

It can be expected that because of the thermal inertia of the recuperator, the proposed cycle will have transient characteristics lying somewhere between an open cycle gas turbine and a combined cycle gas turbine power plant. Studying the effect of using sCO_2 as the working fluid on the life cycle of the power plant components is an active area of research. The operating life is expected to be better than fuel-cell (proton-exchange membrane fuel cell [PEMFC]/solid oxide fuel cell [SOFC])-based systems and not substantially different from comparable conventional gas turbine-based systems. Overall, the thermodynamic analysis of the HYCOS cycle indicates that it could have excellent scaling characteristics. Therefore, unlike conventional gas turbines, it could be scaled down to smaller power output levels (10–50 MWe) without suffering a substantial loss of performance.

EXPERIMENTAL PROCEDURES

Resource availability

Lead contact

Further information and requests for resources should be directed to and will be fulfilled by the lead contact, Arvind Gangoli Rao (a.gangolirao@tudelft.nl).

Materials availability

This study did not generate new unique reagents/materials.

Data and code availability

The source codes of the models used during this analysis are available for download at the 4TU database via https://doi.org/10.4121/d8887792-0e15-4f41-8263-875927562371.

Thermodynamic model

The thermodynamic model used in this analysis was developed in MATLAB. The main assumptions/simplifications used in this model are outlined in this section. Flue gas is treated as an ideal mixture of the main products of $H_2/O_2/CO_2$ combustion (i.e., H_2O and CO_2), while each gaseous component is treated as a real gas. The thermodynamic properties of each of these component gases are obtained from the CoolProp[24] database. Compression and expansion are modeled as adiabatic processes with specified isentropic efficiency. The recuperation process is modeled using the overall heat transfer effectiveness approach which is systematically iterated to achieve the user defined PPTD in the recuperator. The combustion process is simplified to be a purely heat and mass addition process. The knowledge of the flow conditions (temperature, pressure, flow rates) at its inlet and the desired conditions (temperature, pressure) at its outlet reduces the combustion process to a simple energy and mass balance problem which can be solved iteratively. The loss of expansion work caused by turbine cooling is synthetically modeled by injecting 50% of the total turbine cooling flow at the end of the single step block expansion process. The total cooling flow requirement is determined using Gülen's[25] model, which takes into account the dependent variables, namely combustor outlet temperature and cooling flow temperature, in addition to the maximum allowable blade metal temperature, which is a user-defined constant. Last, the fuel and oxidizer are assumed to be stored/available for use in a pre-compressed state at ambient temperature. More details can be found in supplemental experimental procedures.

Combustion model

The combustion model used in this analysis was developed in Ansys Chemkin Pro. It uses the mechanism of Kéromnès et al.[21] to model the combustion chemistry. The choice of this mechanism was based on a literature review and own analysis of different H_2 combustion mechanisms. Several review papers[26–29] that compare the performance of recent H_2/syngas combustions mechanisms have consistently ranked the mechanism of Kéromnès et al. among the best available mechanisms to model H_2 combustion. It was originally designed to model combustion of H_2/CO (syngas) mixtures and therefore is capable of modeling the effect of increased CO_2 concentration in product gases on reactivity of H_2 more accurately as compared with other combustion mechanisms. It consists of 15 species and 48 reactions. When compared with other H_2 and natural gas combustion mechanisms, the mechanism of Kéromnès et al. was found to show the best agreement with experimental results of Sabia and de Joannon[22] in predicting flue gas temperature. The combustion model is based on a simplified reactor network shown in

Figure S1 which is made with two perfectly stirred reactors (PSRs) to represent a staged combustion system. Each PSR is connected to an independent supply line of fuel, oxidizer, and diluent. More details can be found in supplemental experimental procedures.

Thermodynamic model validation

The thermodynamic model was tested by applying it to evaluate the performance of the NET power cycle and comparing the results to the published[19,20] performance data for the cycle. The comparison showed that the present model and the published performance data were in good agreement, with the predicted net cycle efficiency showing a relative deviation of approximately 1%. However, as can be seen from Table S1, a larger deviation was observed in the estimation of the turbine cooling flow requirement, which may be attributed to the simplified treatment of the turbine cooling process in the present model. Nevertheless, since the impact of turbine cooling calculations on the cycle's overall performance is expected to be limited, and the present thermodynamic model is designed to be a low-fidelity tool for analyzing the baseline performance of the HYCOS cycle, this deviation was considered acceptable and the thermodynamic model was considered validated. More details can be found in supplemental experimental procedures.

SUPPLEMENTAL INFORMATION

Supplemental information can be found online at https://doi.org/10.1016/j.xcrp.2023.101514.

ACKNOWLEDGMENTS

The authors received no financial support for the research, authorship, and publication of this article. The authors would like to thank Prof. Rene Pecnik, Delft University of Technology, for his help with the HYCOS cycle graphical abstract.

AUTHOR CONTRIBUTIONS

Conceptualization, A.G.R. and K.D.; Methodology, K.D.; Validation, K.D. and A.G.R.; Investigation, K.D.; Writing – Original Draft, K.D.; Writing – Review & Editing, A.G.R.; Supervision, A.G.R.

DECLARATION OF INTERESTS

The authors declare no competing interests.

INCLUSION AND DIVERSITY

We support inclusive, diverse, and equitable conduct of research.

Received: December 18, 2022
Revised: May 19, 2023
Accepted: June 28, 2023
Published: July 20, 2023

REFERENCES

1. McPherson, M., Johnson, N., and Strubegger, M. (2018). The role of electricity storage and hydrogen technologies in enabling global low-carbon energy transitions. Appl. Energy *216*, 649–661. https://doi.org/10.1016/j.apenergy.2018.02.110.

2. de Sisternes, F.J., Jenkins, J.D., and Botterud, A. (2016). The value of energy storage in decarbonizing the electricity sector. Appl. Energy *175*, 368–379. https://doi.org/10.1016/j.apenergy.2016.05.014.

3. IEA (2014). The Power of Transformation (International Energy Agency). https://doi.org/10.1787/9789264208032-en.

4. Mararakanye, N., and Bekker, B. (2019). Renewable energy integration impacts

within the context of generator type, penetration level and grid characteristics. Renew. Sustain. Energy Rev. *108*, 441–451. https://doi.org/10.1016/j.rser.2019.03.045.

5. Sinsel, S.R., Riemke, R.L., and Hoffmann, V.H. (2020). Challenges and solution technologies for the integration of variable renewable energy sources – a review. Renew. Energy *145*, 2271–2285. https://doi.org/10.1016/j.renene.2019.06.147.

6. Ganzer, C., Pratama, Y.W., and Mac Dowell, N. (2022). The role and value of inter-seasonal grid-scale energy storage in net zero electricity systems. Int. J. Greenh. Gas Control *120*, 103740. https://doi.org/10.1016/j.ijggc.2022.103740.

7. IEA (2022). Global Hydrogen Review 2022 (International Energy Agency). https://doi.org/10.1787/a15b8442-en.

8. IEA (2019). The Future of Hydrogen (International Energy Agency). https://doi.org/10.1787/1e0514c4-en.

9. IRENA (2018). Hydrogen from Renewable Power (International Renewable Energy Agency).

10. Angelino, G. (1968). Carbon Dioxide Condensation Cycles For Power Production. Journal of Engineering for Power *90*, 287–295. https://doi.org/10.1115/1.3609190.

11. Angelino, G. (1969). Real Gas Effects in Carbon Dioxide Cycles. In Proceedings of the ASME 1969 Gas Turbine Conference and Products Show. https://doi.org/10.1115/69-gt-102.

12. Feher, E. (1968). The supercritical thermodynamic power cycle. Energy Convers. *8*, 85–90. https://doi.org/10.1016/0013-7480(68)90105-8.

13. Yantovski, E., Zvagolsky, K., and Gavrilenko, V. (1995). The COOPERATE-demo power cycle. Energy Convers. Manag. *36*, 861–864. https://doi.org/10.1016/0196-8904(95)00139-5.

14. Mathieu, P., and Nihart, R. (1998). Zero Emission MATIANT Cycle. In Proceedings of the ASME 1998 International Gas Turbine and Aeroengine Congress and Exhibition. https://doi.org/10.1115/98-gt-383.

15. Dostal, V., Driscoll, M.J., Hejzlar, P., and Todreas, N.E. (2002). A Supercritical CO2 Gas Turbine Power Cycle for Next-Generation Nuclear Reactors. In Proceedings of the 10th International Conference on Nuclear Engineering. https://doi.org/10.1115/icone10-22192.

16. Allam, R., Palmer, M.R., Brown, G.W., Fetvedt, J., Freed, D., Nomoto, H., Itoh, M., Okita, N., and Jones, C. (2013). High Efficiency and Low Cost of Electricity Generation from Fossil Fuels While Eliminating Atmospheric Emissions, Including Carbon Dioxide. Energy Proc. *37*, 1135–1149. https://doi.org/10.1016/j.egypro.2013.05.211.

17. Zhou, A., Li, X.s., Ren, X.d., Li, X., and Gu, C.w. (2022). Evaluation of the performance and economy for a hybrid energy storage system using hydrogen and compressed carbon dioxide as the energy carrier. Energy Convers. Manag. *264*, 115700. https://doi.org/10.1016/j.enconman.2022.115700.

18. Crespi, F., Gavagnin, G., Sánchez, D., and Martínez, G.S. (2017). Supercritical carbon dioxide cycles for power generation: A review. Appl. Energy *195*, 152–183. https://doi.org/10.1016/j.apenergy.2017.02.048.

19. Scaccabarozzi, R., Gatti, M., and Martelli, E. (2016). Thermodynamic analysis and numerical optimization of the NET Power oxy-combustion cycle. Appl. Energy *178*, 505–526. https://doi.org/10.1016/j.apenergy.2016.06.060.

20. Ferrari, N., Mancuso, L., Davison, J., Chiesa, P., Martelli, E., and Romano, M.C. (2017). Oxy-turbine for Power Plant with CO2 Capture. Energy Proc. *114*, 471–480. https://doi.org/10.1016/j.egypro.2017.03.1189.

21. Kéromnès, A., Metcalfe, W.K., Heufer, K.A., Donohoe, N., Das, A.K., Sung, C.J., Herzler, J., Naumann, C., Griebel, P., Mathieu, O., et al. (2013). An experimental and detailed chemical kinetic modeling study of hydrogen and syngas mixture oxidation at elevated pressures. Combust. Flame *160*, 995–1011. https://doi.org/10.1016/j.combustflame.2013.01.001.

22. Sabia, P., and de Joannon, M. (2020). On H2–O2 oxidation in several bath gases. Int. J. Hydrogen Energy *45*, 8151–8167. https://doi.org/10.1016/j.ijhydene.2020.01.134.

23. Zhang, J., Mi, J., Li, P., Wang, F., and Dally, B.B. (2015). Moderate or Intense Low-Oxygen Dilution Combustion of Methane Diluted by CO_2 and N_2. Energy Fuels *29*, 4576–4585. https://doi.org/10.1021/acs.energyfuels.5b00511.

24. Bell, I.H., Wronski, J., Quoilin, S., and Lemort, V. (2014). Pure and Pseudo-pure Fluid Thermophysical Property Evaluation and the Open-Source Thermophysical Property Library CoolProp. Ind. Eng. Chem. Res. *53*, 2498–2508. https://doi.org/10.1021/ie4033999.

25. Gülen, S.C. (2010). A Simple Parametric Model for the Analysis of Cooled Gas Turbines. J. Eng. Gas Turbines Power *133*. https://doi.org/10.1115/1.4001829.

26. Olm, C., Zsély, I.G., Pálvölgyi, R., Varga, T., Nagy, T., Curran, H.J., and Turányi, T. (2014). Comparison of the performance of several recent hydrogen combustion mechanisms. Combust. Flame *161*, 2219–2234. https://doi.org/10.1016/j.combustflame.2014.03.006.

27. Varga, T., Olm, C., Nagy, T., Zsély, I.G., Valkó, É., Pálvölgyi, R., Curran, H.J., and Turányi, T. (2016). Development of a Joint Hydrogen and Syngas Combustion Mechanism Based on an Optimization Approach. Int. J. Chem. Kinet. *48*, 407–422. https://doi.org/10.1002/kin.21006.

28. Alekseev, V.A., Christensen, M., and Konnov, A.A. (2015). The effect of temperature on the adiabatic burning velocities of diluted hydrogen flames: A kinetic study using an updated mechanism. Combust. Flame *162*, 1884–1898. https://doi.org/10.1016/j.combustflame.2014.12.009.

29. Olm, C., Zsély, I.G., Varga, T., Curran, H.J., and Turányi, T. (2015). Comparison of the performance of several recent syngas combustion mechanisms. Combust. Flame *162*, 1793–1812. https://doi.org/10.1016/j.combustflame.2014.12.001.